

Electron density diagnostic for hot plasmas in coronal regime by using B-like ions

G.Y. Liang^{1,2} and G. Zhao¹

gyliang@bao.ac.cn

ABSTRACT

Line ratio of $3d - 2p$ transition lines in boron-like spectra of Si X, S XII, Ar XIV and Fe XXII has been investigated. Collisional-radiative model calculations reveal that the line ratio is sensitive to the electron density in ranges of $n_e = 4.0 \times 10^7 - 3.0 \times 10^{10} \text{ cm}^{-3}$, $4.0 \times 10^8 - 3.0 \times 10^{11} \text{ cm}^{-3}$, $3.0 \times 10^9 - 4.0 \times 10^{12} \text{ cm}^{-3}$ and $2.0 \times 10^{12} - 3.0 \times 10^{15} \text{ cm}^{-3}$, respectively. This complements the K-shell diagnostics of helium-like ions. By comparison between the prediction and the measured values, effective electron densities in the electron beam ion trap (EBIT) plasmas performed by Lepson and collaborators at Lawrence Livermore EBIT, are estimated to be $n_e = 3.4_{-0.6}^{+0.8} \times 10^{10} \text{ cm}^{-3}$ and $5.6_{-1.1}^{+1.0} \times 10^{10} \text{ cm}^{-3}$ for sulphur and argon plasmas. In case of argon, a good agreement is shown with the actual electron density derived from N VI K-shell spectrum. We further explore the $3d - 2p$ transition lines of Si X and S XII in the stellar coronal spectra measured with the Low Energy Transmission Grating Spectrometer combined with High Resolution Camera on board the *Chandra X-ray Observatory*. The constrained electron densities show a good agreement with the those determined from C V and O VII K-shell spectra.

Subject headings: atomic data – techniques: spectroscopic – stars : coronae – stars: late-type – X-rays : general

1. Introduction

Electron density (n_e) plays an important role in fields of stellar corona, galaxy, interstellar medium of galaxies, clusters of galaxies, as well as the ground tokamak, laser-produced, electron beam ion trap hot plasmas. K-shell spectra (generally refers to the helium-like) shows a powerful diagnostic potential for the electron density. Since the work of Gabriel & Jordan (1969), which defines a ratio between the *forbidden f* line ($1s2s \ ^3S_1 - 1s^2 \ ^1S_0$) and the *intercombination lines i* line ($1s2p \ ^3P_{2,1} - 1s^2 \ ^1S_0$), many literatures reported the ratio by consideration of effects of radiation

¹National Astronomical Observatories, CAS, A20 Datun Road, Chaoyang District, Beijing 100012, China.

²Department of Physics, University of Strathclyde, G1 1XQ Glasgow, United Kingdom

field (Ness et al. 2001), dielectronic and radiative recombinations (Porquet et al. 2001). Porquet et al. (2005) re-investigated the ratio by using updated atomic data of dielectronic and radiative recombinations.

Since the spectra with high-resolution being available, especially the launch of *Chandra* and *XMM-Newton* missions, the ratio of helium-like spectra has been extensively adopted to derived the electron density and further estimations of the stellar structure and the heating mechanism in X-ray emitting regions (Audard et al. 2001; Ness et al. 2002a,b, 2004; Schmitt et al. 2005). Moreover, spatial information of coronae could be assessed indirectly using correlation ($EM = n_e^2 V$, EM refers to an emission measure) between the electron density and the emission measure.

Besides the K-shell emission lines, many L-shell emission lines from highly charged oxygen, neon, silicon, sulphur, calcium, iron and nickel ions have been detected in stellar coronal spectra. For inactive stars, M-shell transition lines were also identified (Raassen et al. 2002). The diagnostic potential of the L-shell emission lines has been investigated by many authors, such as the ratio $I(50.524)/I(50.691)$ of Si X, $I(52.306)/I(43.743)$, $I(52.306)/I(46.391)$ of Si XI addressed in our previous works (Liang & Zhao 2006a; Liang et al. 2006b). Similar characteristics were explored for Si VIII, S X, Ar XIV and Ca XVI etc. (Keenan et al. 1993, 2000, 2001, 2003; Liang et al. 2006c).

For boron-like extreme ultraviolet (EUV) spectra from transitions of $n = 2-2$, Keenan et al. (2000, 2003) studied density-sensitive line ratios of Si X and Ar XIV by using accurate excitation data from R -matrix method. For $3d - 2p$ transition lines spanned in the soft X-ray region, line intensity ratios of highly charged silicon ions were investigated in our previous work (Liang et al. 2006b), which shows a n_e -sensitivity in the range of $n_e = 4.0 \times 10^7 - 3.0 \times 10^{10} \text{ cm}^{-3}$. By laboratory measurements in the electron beam ion trap (EBIT), Chen et al. (2004) test the density-sensitive line ratios of Ar XIV and Fe XXII in ranges of $n_e = 2.0 \times 10^{10} - 1.0 \times 10^{12} \text{ cm}^{-3}$ and low-density limit around $1.0 \times 10^{12} \text{ cm}^{-3}$, respectively. In that work, the actual electron density was constrained from K-shell N VI spectrum. However, the diagnostic application of emission lines of S XII have not been investigated to our best knowledge, though its two lines at 36.398 and 36.564 Å have been identified for inactive star—Procyon.

In this work, we make a systematically analyses for the $3d - 2p$ density-sensitive transition lines of boron-like spectra including Si X, S XII, Ar XIV and Fe XXII based on the collisional-radiative model as given in Sec. 2. In Sec. 3, we explore the $3d - 2p$ transition lines of S XII at 36.398 and 36.564 Å in the stellar coronal spectra observed by the low energy transmission grating (LETG) spectrometer on board the *Chandra X-ray observatory*. Furthermore, the electron densities of stellar corona and laboratory plasmas produced in the EBIT are estimated as illustrated in Sec. 4, followed by conclusions outlined in Sec. 5.

2. Theory

2.1. $3d-2p$ transition lines

The line intensity ratio between the $3d\ ^2D_{5/2}-2p\ ^2P_{3/2}$ transition and the $3d\ ^2D_{3/2}-2p\ ^2P_{1/2}$ transition lines are known to be sensitive to the electron density but on the other hand rather insensitive to the electron temperature. This feature follows from the fact that the upper level is populated mainly by collisional excitation from the density-sensitive lower metastable level. In the following paragraph, we take S XII to explain this property.

As shown in Fig. 1, the levels of the configuration $2s2p^2$ have the largest excitation rate from the levels of the ground configuration, whereas the decaying lines span in the EUV wavelength region. Here we pay special attention on the X-ray emission lines. The $3d\ ^2D_{5/2}$ level has a high excitation rate from and decay rate to the metastable $2p\ ^2P_{3/2}$ level, which is forbidden to decay to the ground state. By increasing the electron density, a significant fraction of the $^2P_{3/2}$ population can be re-excited to the $^2D_{5/2}$ state, from where it relaxes to the $^2P_{3/2}$ state and, therefore, the line intensity at $36.564\ \text{\AA}$ increases. On the other hand, by the depopulation of the ground state $^2P_{1/2}$ due to the shelving of electrons in the metastable level, the excitation of the resonance line ($3d\ ^2D_{3/2}-2p\ ^2P_{1/2}$) at $36.398\ \text{\AA}$ of S XII decreases at high densities.

It is clear that the $2s3d\ ^2D_{3/2}$ level can also decay to the metastable $^2P_{3/2}$ level with a low branching ratio. However, as this transition line (at $36.573\ \text{\AA}$ for S XII) can not be resolved from the $36.564\ \text{\AA}$ line due to the limited spectral resolution in the present space missions, we have to take into account this blend effect. Since the $3d\ ^2D_{3/2}$ is directly populated from the ground state, the intensity of $36.573\ \text{\AA}$ has a similar dependence on n_e as the $36.398\ \text{\AA}$ resonance line and its relative contribution to the blended $36.564\ \text{\AA}$ line becomes dominant at low electron density.

2.2. Calculation of the line ratio

Adopting a collisional-radiative model, we calculated the line ratio $[I(3d_{5/2} - 2p_{3/2}) + I(3d_{3/2} - 2p_{3/2})] / I(3d_{3/2} - 2p_{1/2})$ of Si X, S XII, Ar XIV and Fe XXII, as a function of the electron density for a Maxwellian electron distribution at temperatures of peak fraction of these ions in the work of Bryans et al. (2006). The transition wavelengths are listed in Table 1. For Si X and Ar XIV, the atomic data including energy levels, radiative decay rates and impact excitation rates are from our detailed calculation. Some excitation data within $n = 2 - 2$ transitions are replaced by more accurate calculation with R -matrix method as explained in previous literatures (Liang et al. 2006b,c). For S XII and Fe XXII, we adopt the CHIANTI package of the new version 5.2. In this code, the atomic data is updated recently as depicted by Landi et al. (2006). For S XII, the electron impact excitation data of Zhang et al. (1994) has been adopted, in which small errors found by later have been corrected by authors in the present version of the CHIANTI. Resonance effects for excitations among the lowest 15 fine-structure levels have been included by the R -matrix

method. For Fe XXII, the electron excitation data between the lowest 204 levels are from the work of Badnell et al. (2001) who adopted close-coupling R -matrix method and in conjunction with intermediate-coupling frame transformation method. The electron excitation data between higher 205-513 levels adopts the calculation of Landi & Gu (2006), in which the resonance effects were considered by an isolated-resonance approximation. Above the ionization energy, the calculation of Bautista et al. (2004) with the Breit-Pauli R -matrix method was used. Additionally, proton excitations between the fine-structure states of the ground configuration and $2s2p^2\ ^4P$ term were also included (Foster et al. 1997) in the CHIANTI. In this work, close-coupled impact-parameter method was used.

Figure 2 shows the prediction of the line ratio at temperatures of $\log T_e=6.1$ K for Si X, 6.3 K for S XII, 6.5 K for Ar XIV and 7.1 K for Fe XXII. This demonstrates that the ratio is sensitive to the electron density in ranges $n_e = 4.0 \times 10^7 - 3.0 \times 10^{10} \text{ cm}^{-3}$, $4.0 \times 10^8 - 3.0 \times 10^{11} \text{ cm}^{-3}$, $3.0 \times 10^9 - 4.0 \times 10^{12} \text{ cm}^{-3}$ and $2.0 \times 10^{12} - 3.0 \times 10^{15} \text{ cm}^{-3}$ for Si X, S XII, Ar XIV and Fe XXII, respectively. We further calculate the ratio in the temperature ranges $\log T_e=6.0-6.2$ K for Si X, 6.1–6.4 K for S XII, 6.4–6.6 K for Ar XIV and 7.0–7.2 K for Fe XXII, as illustrated by hatched regions in Fig. 2, which reveals that the ratio is insensitive to the electron temperature. This indicates that the ratio $[I(3d_{5/2} - 2p_{3/2}) + I(3d_{3/2} - 2p_{3/2})] / I(3d_{3/2} - 2p_{1/2})$ is a good n_e -diagnostic method for hot plasmas, and compensates the K-shell spectra.

3. Observations

The wavelength range spanned by the $3d - 2p$ transition lines of the present interested boron-like ions, is covered by the High and Medium Energy Grating (HEG and MEG) spectrometers, the Low Energy Transmission Grating (LETG) spectrometer on board *Chandra*, as well as the Reflection Grating Spectrometer (RGS) on board *XMM-Newton* with high-resolution. One specific advantage of LETG observations results from its large wavelength coverage in one spectrum, that is the $3d - 2p$ lines (see Table 1) of the interested ions can be detected at the same time.

Our sample consists of 6 stars including two normal dwarf stars, i.e., Procyon and α Cen B, an active late-type dwarf star, ϵ Eri, two active binary systems, Capella and YY Gem, and an pre-main sequence late-type star–TW Hya. The properties of our sample, along with ObsID and exposure time are summarized in Table 2. All observations adopt grating of LETG combined with High Resolution Camera (HRC) instrument on board *Chandra* Observatory. In case of Capella, an additional observation (with ObsID=55) with Advanced CCD Imaging Spectrometer (ACIS)-S instrument is used. Because ACIS-S instrument has significant energy resolution to separate overlapping spectral orders, LETG+ACIS-S observations are better choice for determination of the electron density. However only one observation is available from *Chandra Data Archival Center* for our sample. Another goal of analysis for the ACIS-S spectrum of Capella is to validate whether there is significant contamination from high-order (refer to $m \geq 2$) spectra around the selected lines (36.398 and 36.564 Å). If line fluxes derived from the two different observations are comparable,

no contamination from high-order spectra can be concluded. Reduction of the LETG datasets uses CIAO3.3 software with the science threads for LETGS/HRC-S observations. Figure 3 shows the spectra for Procyon, α Cen B, Capella, ϵ Eri, YY Gem and TW Hya in the wavelength range of 36.0–37.0 Å.

The $3d-2p$ transition lines of Si X have been identified and explained in detail by Liang & Zhao (2006a). Argon is an underabundant element in stellar corona, and no emission lines of Ar XIV have been identified so far. Iron is an abundant elements in astrophysical environment. However, the $3d-2p$ resonance line at 11.769 Å is contaminated by the Fe XXIII line at 11.738 Å for Capella (Behar et al. 2001). Here, we pay a special attention on the identification of $3d-2p$ lines of S XII at 36.398 Å and 36.564 Å as shown in Fig. 3.

4. Results and Discussions

4.1. line fluxes of $3d-2p$ transitions of S XII

Line fluxes are determined by modelling the spectra locally with narrow Gaussian profiles and constant value representing background and (pseudo-)continuum emissions determined in line-free region. The observed line width is about 0.06 Å over the interested region, which is comparable with the broadening of instrument for point-like source. The fluxes have been obtained after correction for the effective area as listed in Table 3.

For Procyon, the two transition lines have been identified by Raassen et al. (2002) in the RGS and LETG observations. Here the line fluxes are derived separately again for the co-added LETG observations, which shows a good agreement with results of Raassen et al. (2002) within 1σ error as illustrated in Table 3. For other stars, no reports of the identifications for the two lines can be found to our best knowledge.

For Capella, we fit the HRC-S and ACIS-S observations separately with multi-Gaussian components as detailed illustration in Fig. 4. It is clear that the line-width in HRC-S observation is wider than ACIS-S observation, which is due to its lower resolution. Additionally, for the line at 36.398 Å, the derived line flux from HRC-S observation is higher than the value from ACIS-S observation by a factor of ~ 2.8 (see Table 3). This is due to the contamination from third-order diffraction of emission line at ~ 12.136 Å with flux of $11.04 \pm 0.30 \times 10^{-4}$ photons $\text{cm}^{-2}\text{s}^{-1}$ (see 7-th column in Table 3), resulting from Ne X Ly α (12.134 Å) and Fe XVII (12.124 Å). According to the line fluxes around 36.394 Å derived from HRC and ACIS observations as well as the line flux around 12.136 Å, we conclude that the efficiency of third-order diffraction is about $(17.4 \pm 8.2)\%$ at the local wavelength range. The different background levels are due to the different effective areas (6.24 and 8.43 cm^2 , respectively). A search from the APEC/APED v1.3.1 (Smith et al. 2001) indicates that another emission line from Fe XVII at 36.358 Å partially blends in the HRC-S observation. For the emission line around 36.564 Å, the fitting result in the HRC-S observation is

also higher than the value derived from ACIS-S observation by a factor of ~ 1.6 . This is due to the blending from Fe XVII line at 36.692 Å as resolved in case of ACIS-S observation. Here a question appears that whether there is a similar blending effect from high-order diffraction for inactive stars such as Procyon and α Cen B. Analysis indicates that no emission line is detected at ~ 12.136 Å for the inactive stars, that is, there is no contamination from third-order diffraction at the emission line at 36.394 Å.

For other three stars including ϵ Eri, YY Gem and TW Hya, similar procedure is used. The resulting line fluxes are listed in Table 3. However the blending effect has not been extracted. The line flux of the first order diffraction at 12.136 Å is listed in the 7-th column of Table 3, which will be used for the extraction of its contribution at the third-order diffraction position.

4.2. n_e -diagnostic from the ratio

The diagnostic results of n_e from Si X for stellar corona have been reported in our previous work (Liang et al. 2006b). Here the observed ratio and the constrained electron density with 1σ errors are overlaid again in Fig. 2 (see black symbols). The comparison with the diagnosed electron density from K-shell C V ions, shows a good consistency, and a better results with low error bars for inactive stars (see the black symbols in Fig. 2).

Using the line fluxes derived in the above section, we diagnose the electron density for our sample (see the blue symbols in Fig. 2) as listed in Table 4. For Capella, we adopt the line flux from ACIS-S observation, whereas the line fluxes from the HRC-S observations are used for other stars in our sample, that is the blending effect has not been considered. The deduced densities are typical values for inactive stars. We further compare the densities with the values derived from spectra of helium-like ions with the same peak line formation temperatures in the ionization equilibrium (Bryans et al. 2006) as shown in Fig. 5.

The density from Si X shows a good agreement with the value constrained by C V within the statistical errors. For ϵ Eri and α Cen B, electron densities are not available from the helium-like C V and O VII spectra, respectively. The diagnostic from boron-like Si X and S XII compensates the estimation for the X-ray emitting regions with low temperatures. For inactive stars and Capella, the density constrained by S XII is also in agreement with the results from O VII. However, for ϵ Eri, YY Gem and TW Hya, it is clear that the density constrained by S XII is lower than the result from O VII, which is due to the blending effect from third order diffraction of the emission line at 12.136 Å resulting from Fe XVII and Ne X. For pre-main sequence star—TW Hya, Stelzer & Schmitt (2004) estimated the electron density is not less than $1.0 \times 10^{12} \text{cm}^{-3}$, and conclude the X-ray emission being from the accretion shock.

Adopting the efficiency of third order diffraction determined in above subsection, and the line flux at 12.136 Å, we extract its contribution around 36.394 Å, and re-derived the line ratio and the corresponding electron density as illustrated by open-symbols in Fig. 4. For ϵ Eri, the resulted

electron density is still lower than the value constrained by O VII by an order of magnitude. However, the determined n_e from S XII shows an agreement with the n_e constrained by O VII for YY Gem and TW Hya within the 1σ uncertainty. We also notice that the electron density determined from S XII (or O VII) is slightly higher than that from Si X (or C V) with lower peak line formation temperature.

By using the line ratio of S XII and Ar XIV, effective electron densities of the laboratory plasmas in the Lawrence Livermore EBIT performed by Lepson and collaborators (Lepson et al. 2003, 2005), are constrained by the boron-like line ratio as illustrated by the red-square symbols in Fig. 2. For argon plasma, the constrained electron density ($5.6_{-1.1}^{+1.0} \times 10^{10} \text{ cm}^{-3}$) agrees well with the actual density ($6.0 \times 10^{10} \text{ cm}^{-3}$) estimated by the K-shell N VI spectrum as reported by Chen et al. (2004). For sulphur plasma, the electron density is firstly estimated to be $3.4_{-0.6}^{+0.8} \times 10^{10} \text{ cm}^{-3}$. Through the laboratory measurement, Chen et al. (2004) further benchmark the line ratio of Fe XXII at the low-density limit. The experimental values are overlapped again by the red-circle symbols in Fig. 2. The astrophysical ratio (dark-yellow triangle) of Fe XXII is derived for the ACIS-S observation of Capella, and shows the constrained electron density is less than $7.6 \times 10^{12} \text{ cm}^{-3}$, which is consistent with previous works for the stellar corona.

5. Conclusions

Collisional-radiative model calculation reveals that the line ratio $[I(3d_{5/2} - 2p_{3/2}) + I(3d_{3/2} - 2p_{3/2})] / I(3d_{3/2} - 2p_{1/2})$ of Si X, S XII, Ar XIV and Fe XXII is sensitive to the electron density in the ranges $n_e = 4.0 \times 10^7 - 3.0 \times 10^{10} \text{ cm}^{-3}$, $4.0 \times 10^8 - 3.0 \times 10^{11} \text{ cm}^{-3}$, $3.0 \times 10^9 - 4.0 \times 10^{12} \text{ cm}^{-3}$ and $2.0 \times 10^{12} - 3.0 \times 10^{15} \text{ cm}^{-3}$, respectively. This compensates the n_e -diagnostics of K-shell spectra, e.g. helium-like ions. We further explore the $3d - 2p$ transition lines of boron-like ions in the stellar coronal spectra measured with the LETG Spectrometer combined with HRC on board the *Chandra X-ray Observatory*. Though the emission lines are very weak, the electron density constrained from these lines, shows a good agreement with the those constrained by C V and O VII K-shell spectra inactive stars, and the uncertainties can be comparable with and even better than those estimated from K-shell spectra. When the blending effect from third-order diffraction has been taken into account, the deduced electron density increases, and gets a better consistency with that estimated from O VII for active stars, e.g. YY Gem. We also notice that the determined electron density from S XII is higher than that constrained from Si X, which is due to its higher peak temperature of line formations in collisional equilibrium.

By using the line ratio, effective electron densities in the electron beam ion trap (EBIT) plasma performed by Lepson et al. (2003, 2005) at Lawrence Livermore EBIT, are constrained to be $n_e = 3.4_{-0.6}^{+0.8} \times 10^{10} \text{ cm}^{-3}$ and $5.6_{-1.1}^{+1.0} \times 10^{10} \text{ cm}^{-3}$ for sulphur and argon plasmas. In case of argon, a good agreement is found with the actual electron density derived from N VI K-shell spectrum.

In conclusion, the boron-like $3d - 2p$ spectra provides a good n_e -diagnostics for hot plasmas, and compensates the spectral diagnostic of K-shell spectrum.

G.Y. thanks Prof. Badnell, University of Strathclyde in United Kingdom, for his constructive suggestions. This study is supported by the National Natural Science Foundation of China under Grant Nos. 10603007, 10521001 and 10573024, as well as the National Basic Research Program of China (973 program) under grant No. 2007CB815103.

REFERENCES

- Audard M., Behar E., Güdel M., et al., 2001, *A&A*, 365, L329
- Badnell N.R., Griffin D.C., & Mitnik D.M., 2001, *J. Phys. B: At. Mol. Opt. Phys.*, 34, 5071
- Bautista M.A., Mendoza C., Kallman T.R., & Palmeri P., 2004, *A&A*, 418, 1171
- Behar E., Cottam J., Kahn S. M., et al., 2001, *ApJ*, 548, 966
- Bryans P., Badnell N.R., Gorczyca T.W., et al., 2006, *ApJS*, 167, 343
- Chen H., Beiersdorfer P., Heeter L.A., Liedahl D.A., Naranjo-Rivera K.L., Träbert E., Gu M.F., & Lepson J.K., 2004, *ApJ*, 611, 598
- Foster V.J., Keenan F.P., & Reid R.H.G., 1997, *At. Data and Nucl. Data Tables*, 69, 77
- Gabriel A.H. & Jordan C., 1969, *MNRAS*, 145, 241
- Kastner J.H., Huenemoerder D. P., Schulz N.S., et al. 2002, *ApJ*, 567, 434
- Keenan F.P., Conlon E.S., Foster V.J., et al., 1993, *Sol. Phys.*, 145, 291
- Keenan F.P., Pinfield D.J., Mathioudaskis M., et al., 2000, *Sol. Phys.*, 197, 253
- Keenan F.P., Aggarwal K.M., Katsiyannis A.C., et al., 2003, *Sol. Phys.*, 217, 225
- Keenan F.P., Katsiyannis A. C., Reid R.H.G., Pradhan A.K., Zhang H.L. & Widing K.G., 2003, *MNRAS*, 346, 58
- Keenan F.P., Aggarwal K.M., Williams D.R., et al., 2001, *MNRAS*, 326, 1387
- Keenan F.P., O’Shea E., Thomas R.J., et al., 2000, *MNRAS*, 315, 450
- Landi E., Del Zanna G., Young P.R., et al., 2006, *ApJS*, 162, 261
- Landi E., & Gu M.F, 2006, *ApJ*, 640, 1171
- Lepson J.K., Beiersdorfer P., Behar E., et al., 2003, *ApJ*, 590, 604

- Lepson J.K., Beiersdorfer P., Behar E., et al., 2005, ApJ, 625, 1045
- Liang G.Y., Zhao G., 2006a, AJ, 132, 1547
- Liang G.Y., Zhao G., Shi J.R., 2006b, AJ, 132, 371
- Liang G.Y., Zhao G., & Zeng J. L. & Shi J.R., 2006c, J. Quant. Spect. of Rad. Trans., 102, 473
- Ness J.-U., Brickhouse N. S., Drake J.J., & Huenemoerder D. P., 2003, ApJ, 598, 1277
- Ness J.-U., Güdel M., Schmitt J.H.M.M., Audard M., & Telleschi A., 2004, A&A, 427, 667
- Ness J.-U., Mewe R., Schmitt J.H.M.M., et al., 2001, A&A, 367, 282
- Ness J.-U., Schmitt J.H.M.M., Burwitz V., et al., 2002a, A&A, 394, 911
- Ness J.-U., Schmitt J.H.M.M., Burwitz V., et al., 2002b, A&A, 387, 1032
- Ness J.-U., & Schmitt J. H.M.M., 2005, A&A, 444, L41
- Porquet D., Mewe R., Dubau J., et al., 2001, A&A, 376, 1113
- Raassen A.J.J., Mewe R., Audard M., et al., 2002, A&A, 389, 228
- Raassen A.J.J., Ness J.-U., Mewe R., et al., 2003, A&A, 400, 671
- Schmitt J.H.M.M., Robrade J., Ness J.-U., et al., 2005, A&A, 432, L35
- Stelzer B., & Schmitt J.H.M.M., 2004, A&A, 418, 687
- Smith, R.K., Brickhouse, N.S., Liedahl D. A., et al. 2001, ApJ, 556, L91
- Zhang H.L., Graziani M., Pradhan A.K., 1994, A&A, 283, 319

This preprint was prepared with the AAS L^AT_EX macros v5.2.

Table 1: Wavelengths of three interested $3d-2p$ transitions of Si X, S XII, Ar XIV and Fe XXII.

Transitions	Wavelength (Å)			
	Si X	S XII	Ar XIV	Fe XXII
$2s^23d\ ^2D_{3/2} - 2s^22p\ ^2P_{1/2}$	50.524	36.398	27.469	11.769
$2s^23d\ ^2D_{5/2} - 2s^22p\ ^2P_{3/2}$	50.691	36.564	27.629	11.921
$2s^23d\ ^2D_{3/2} - 2s^22p\ ^2P_{3/2}$	50.703	36.573	27.642	11.936

Table 2: Summary of stellar properties and X-ray luminosity (5–175 Å) for the stars.

star	ObsID	$t_{\text{obs}}^{\text{a}}$ ks	SpectralType	distance ^b pc	$T_{\text{eff}}^{\text{a}}$ K	$\log(L_{\text{bol}})$ erg/s	R_{\star}^{b} [R_{\odot}]	L_{X}^{c} 10^{28} erg/s
Procyon	63 + 1224 + 1461	70.15 + 20.93 + 70.25	F5.01V – V	3.5	6540	34.46	2.06	2.43
α Cen B	29	79.5	K0.0V	1.34	5780	33.28	0.8	0.52
Capella	1248/55	84.7/53.48	G1.0III/K0.0I	12.94	5850	35.71	9.2/13	255
ϵ Eri	1869	105.3	K2.0V	3.22	4780	33.11	0.81	20.9
YY Gem	28	57.63	dM1e/dM1e	14.7			0.66/0.58	54.4
TW Hya	6443	150.24	K8V	56.0				150.0 ^d

^a Exposure time of observation

^b From Ness et al. (2004)

^c From Ness et al. (2002a)

^d Derived from *XMM*-Newton observation (Stelzer & Schmitt 2004).

Table 3: Measured flux (in unit of 1.0×10^{-4} photon $\text{s}^{-1} \text{cm}^{-2}$) of S XII lines at 36.398 Å and 36.564 Å and the line at 12.136 Å for 6 stars observed with the LETG spectrometer. F^- and F^+ indicate the line fluxes with 1σ error derived from negative and positive diffraction spectra, respectively.

Stars	Instrument	$F^-(36.398\text{\AA})$	$F^+(36.398\text{\AA})$	$F^-(36.564\text{\AA})$	$F^+(36.564\text{\AA})$	$F(12.136\text{\AA})$
Procyon	HRC – S	0.38 ± 0.11	0.33 ± 0.13	0.24 ± 0.11	0.32 ± 0.13	–
Procyon ^a	HRC – S	0.34 ± 0.14	–	0.24 ± 0.13	–	–
Procyon ^a	RGS1	0.35 ± 0.10	–	0.15 ± 0.06	–	–
Procyon ^a	RGS2	0.28 ± 0.07	–	0.29 ± 0.09	–	–
α Cen B	HRC – S	0.43 ± 0.11	–	0.32 ± 0.11	–	–
Capella	HRC – S	2.61 ± 0.89	2.84 ± 0.87	0.89 ± 0.23	0.91 ± 0.24	11.04 ± 0.30
Capella	ACIS	0.69 ± 0.14	–	0.34 ± 0.14	–	–
ϵ Eri	HRC – S	0.71 ± 0.13	0.78 ± 0.15	0.23 ± 0.11	0.45 ± 0.13	0.91 ± 0.04
YY Gem	HRC – S	0.29 ± 0.06	0.49 ± 0.09	0.15 ± 0.07	0.19 ± 0.09	1.03 ± 0.07
TW Hya	HRC – S	0.37 ± 0.10	0.42 ± 0.11	0.36 ± 0.10	0.13 ± 0.09	0.48 ± 0.03

^a The line fluxes in this case are from Raassen et al. (2002).

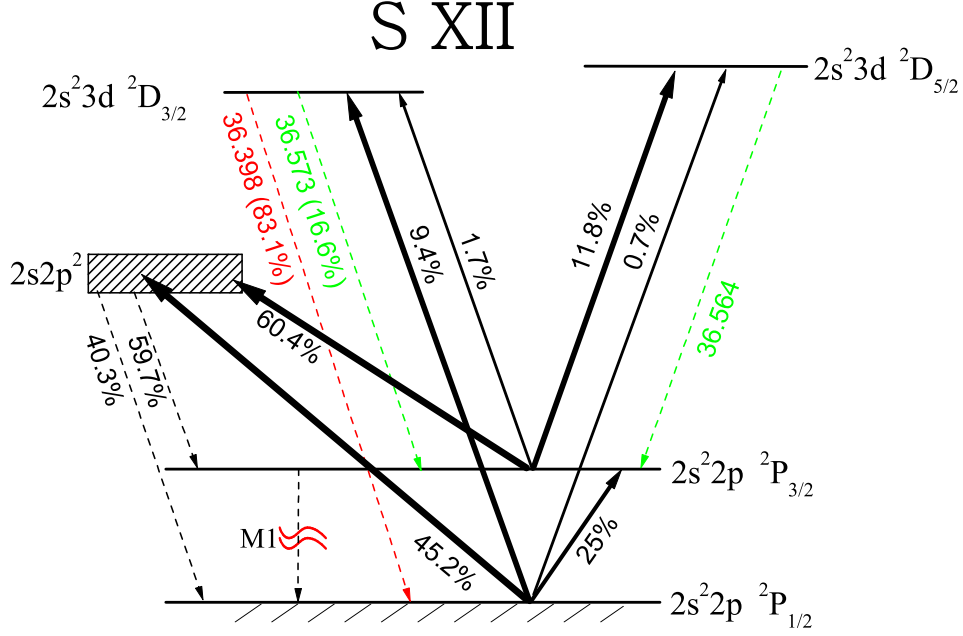


Fig. 1.— (Color online) Scheme of the processes responsible for the sensitivity of the $n = 3 \rightarrow n = 2$ transitions (see red- and green-dashed lines) in S XII against the electron density. Wavelengths (in Å) and radiative branching fractions different from 100% are indicated for the radiative transitions (dashed lines). Relative magnitudes of collisional excitation strength are given in percent as well as represented by the thickness of the corresponding solid lines.

Table 4: Diagnosed electron densities (in unit of cm^{-3}) from Si X and S XII for our sample.

Stars	$n_e(\text{Si X})$	$n_e(\text{S XII})$
Procyon	$4.2^{+2.9}_{-1.6} \times 10^8$	$2.5^{+4.7} \times 10^9$
α Cen B	$4.0^{+5.8}_{-2.1} \times 10^8$	$4.1^{+3.9}_{-3.3} \times 10^9$
Capella	$2.0^{+4.0} \times 10^9$	$1.3^{+2.0} \times 10^9$
ϵ Eri	$1.3^{1.8}_{-1.2} \times 10^9$	$1.0^{+10.2} \times 10^8$
YY Gem	–	$1.5^{+3.0}_{-0.8} \times 10^9$
TW Hya	–	$7.1^{+9.1}_{-4.9} \times 10^9$

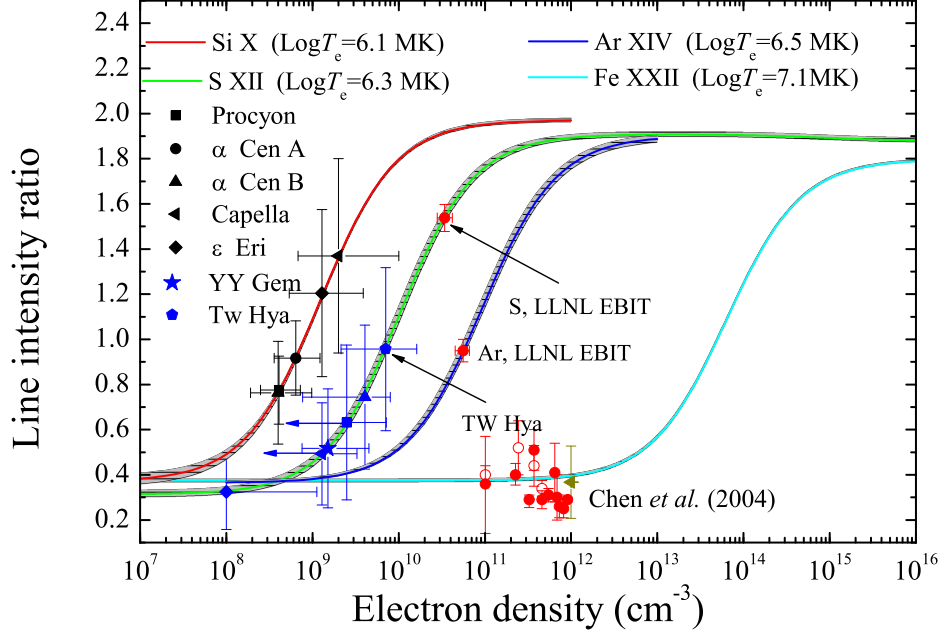


Fig. 2.— (Color online) Line intensity ratio, $[I(3d_{5/2} - 2p_{3/2}) + I(3d_{3/2} - 2p_{3/2})] / I(3d_{3/2} - 2p_{1/2})$ of Si X, S XII, Ar XIV and Fe XXII, as a function of the electron density for a Maxwellian electron distribution at temperatures of peak fraction of these ions in the work of Bryans et al. (2006) (see the legend). The hatched areas indicate predictions for thermal plasmas in the temperature range (in $\log T_e$) of 6.0–6.3 K for Si X, 6.2–6.4 K for S XII, 6.4–6.6 K for Ar XIV and 7.0–7.2 K for Fe XXII. Black symbols with error bars are the observed line ratios of Si X in the stellar corona. Blue symbols with error bars are the observed line ratios of S XII in the stellar corona. The red-square symbols with error bars are the laboratory measured ratios of S XII and Ar XIV in the works of Lepson et al. (2003, 2005). The red-circle symbols in range of $n_e = 10^{11} - 10^{12} \text{ cm}^{-3}$ are extracted from the work of Chen et al. (2004), which represent the measured ratios and electron densities in the EBIT experiments, whereas the dark-yellow triangle symbol denotes the ratio of Fe XXII lines extracted from ACIS-S observation for Capella.

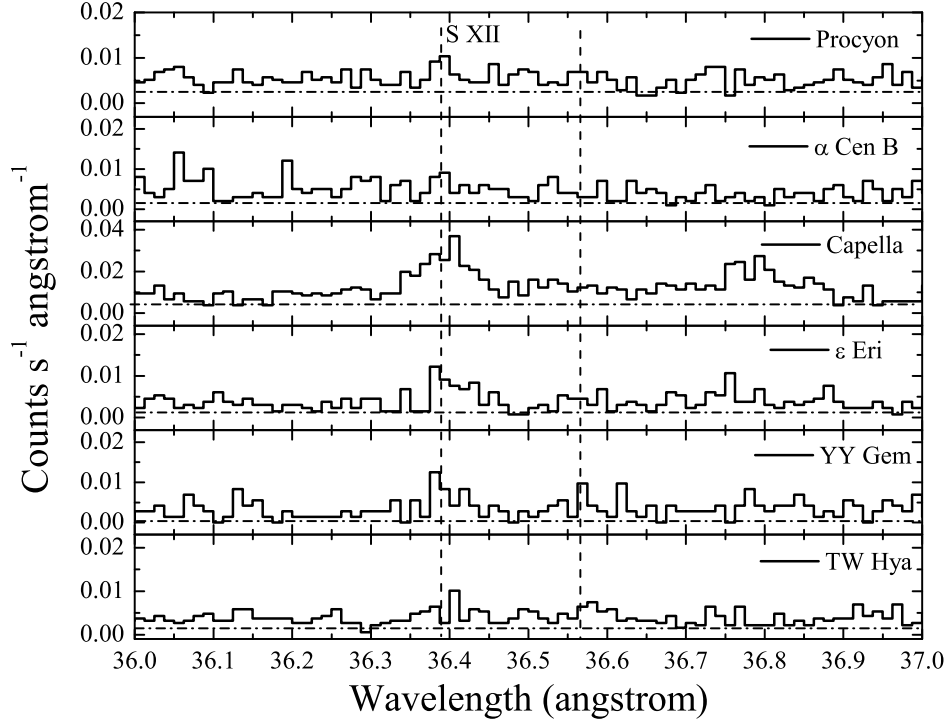


Fig. 3.— Extracted LETGS spectra of our sample in the wavelength range 36.0–37.0 Å. The HRC-S instrument was used for all observation. The prominent lines from S XII are labelled by dashed vertical lines. The dash-dotted horizontal lines refer to the continuum levels for each star.

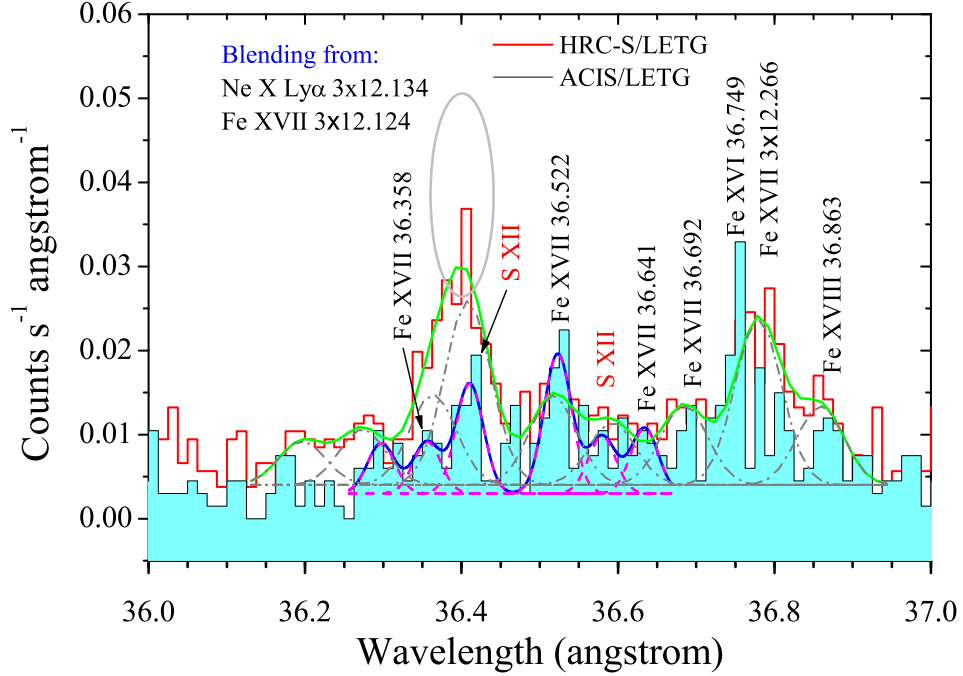


Fig. 4.— (Color online) Observed spectra (step lines) of Capella in wavelength range of 36.0—37.0 Å and their Gaussian fittings (smooth lines) around S XII lines (marked by red labels) from $2s^23d\ ^2D_{3/2}-2s^22p\ ^2P_{1/2}$ transition at 36.398 Å and $2s^23d\ ^2D_{3/2,5/2}-2s^22p\ ^2P_{3/2}$ transitions at 36.574 and 36.564 Å. Blending from lines of higher-order diffractions are resolved out by the ACIS instrument (see black-step curve with filled area), whereas it can not be resolved out by the HRC-S instrument (see red-step curve).

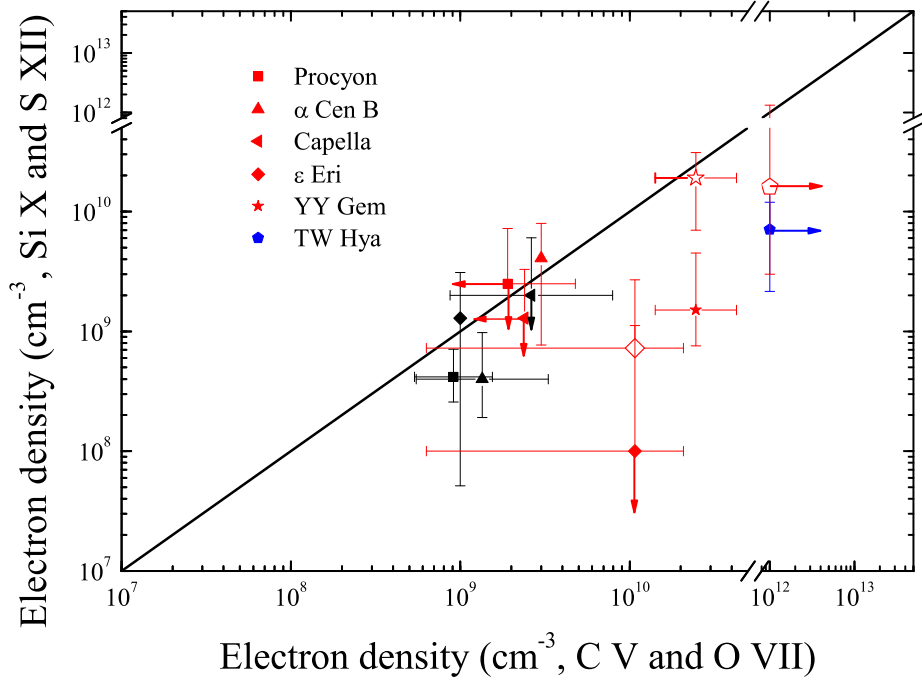


Fig. 5.— (Color online) Comparisons of the electron densities derived from K-shell ions (C V and O VII) and boron-like ions (Si X and S XII). Black symbols denote results from C V and Si X; red symbols refer to results from O VII and S XII. The linear line indicates the same densities from the K-shell and boron-like spectra. Symbols without error bars and arrows indicate no electron density being available. For ϵ Eri, YY Gem and TW Hya, taking the third-order diffraction into account, the resulted electron density is shown by red-opened symbols.